Pathways of Infusate Loss During Convection Enhanced Delivery into the Putamen Nucleus

Martin L. Brady[1], **Raghu Raghavan**[1], **Andrew Alexander**[2,3,4], **Ken Kubota**[7], **Karl Sillay**[5], and **Marina E. Emborg**[3,6]

[1]Therataxis LLC, Baltimore, MD 21218, USA

[2]Waisman Center, University of Wisconsin, Madison, WI 53715, USA

[3]Departments of Medical Physics Wisconsin National Primate Research Center, University of Wisconsin, Madison, WI 53715, USA

[4]Departments of Psychiatry Wisconsin National Primate Research Center, University of Wisconsin, Madison, WI 53715, USA

[5]Departments of Neurosurgery Wisconsin National Primate Research Center, University of Wisconsin, Madison, WI 53715, USA

[6]Preclinical Parkinsons Research Program, Wisconsin National Primate Research Center, University of Wisconsin, Madison, WI 53715, USA

[7]Kinetics Foundation, Los Altos, CA 94022, USA

Abstract

Background—New strategies aiming to treat Parkinson's disease such as delivery of trophic factors via protein infusion or gene transfer depend upon localized intracerebral infusion, mainly into the putamen nucleus. Convection enhanced delivery (CED) has been proposed as method to improve intracerebral distribution of therapies. Yet analysis of controversial results during the clinical translation of these strategies suggests that intracerebral misdistribution of infusate may have affected the outcomes by limiting the amount of treatment into the target region.

Objectives—This study aimed to identify possible pathways of infusate loss and their relative impact in the success of targeted CED into the postcommisural ventral putamen nucleus.

Methods—Thirteen adult macaque monkeys received under intraoperative magnetic resonance imaging (MRI) guidance, intraputaminal CED infusions of 100 µl of 2.0 mM gadoteridol and bromophenol blue (0.16 mg/ml) solution at a rate of 1.0 µl/min. Quantitative maps of infusate concentration were computed at 10 minute intervals throughout the procedure in a 3T MRI. The fraction of tracer lost from the putamen and as well as the path of loss was evaluated and quantified for each infusion.

Results—All injections (total 22) were successfully placed in the ventral postcommisural putamen nucleus. Four major paths of infusate loss from the putamen were observed: *overflow* across putamen boundaries, *perivascular flow* along large blood vessels, *backflow* along the inserted catheter and *catheter tract leakage* into the vacated catheter tract upon catheter removal. Overflow loss was observed within the first 30 µl of infusion in all cases. Measurable tracer loss following the path of an artery out of the putamen was observed in 15 cases, and in eight of these cases the loss was greater than 10% of infusate. Backflow that exited the putamen was observed in

Corresponding Author: Martin Brady Therataxis, LLC 1101 E. 33rd Street, Ste. B305, Baltimore, MD 21218 (443) 451-7156 (phone); (443) 451-7157 (fax) mbrady@therataxis.com.

4 cases and led to large loss of infusate (80% in one case) into the corona radiata. Loss into the vacated catheter tract amounted only to a few µl.

Conclusions—Our analysis demonstrate that after controlling for targeting, catheter type, infusion rate and infusate, the main issues during surgical planning are the identification of appropriate infusate volume that matches the target area, as well as mapping the regional vasculature as it may become a pathway for infusate loss. Most importantly, these results underscore the significance of presurgical planning for catheter placement and infusion and the value of imaging guidance to ensure targeting accuracy.

Keywords

Parkinson's disease; convection-enhanced delivery; intraputaminal infusion; magnetic resonance imaging

Introduction

The putamen nucleus has been identified as a target for novel strategies involving intraparenchymal delivery of protein and gene therapies for Parkinson's disease [1,2,3,4,5]. While there have been several Phase I clinical trials that suggest possible efficacy of trophic factors infused directly into the putamen [4,6,7], the efficacy of these strategies has not been confirmed in a controlled Phase II study [1,2]. Inadequate delivery has been speculated to be a possible factor for the failure of these trials. For example, it has been suggested that the failure of a phase II trial for delivery of glial derived neurotrophic factor (GDNF) was due to variations in catheter placement that affected protein distribution and diminished availability to the target [8]. The importance of appropriate target coverage is further highlighted in a report of the post mortem analysis of two patients that were part of a Phase II clinical gene therapy trial to assess the effect of adenoassociated virus serotype 2/2 (AAV2) encoding for the neurotrophic factor neurturin. The investigators described that despite the patients receiving eight AAV2 neurturin inoculations spread across the putamen, only 15% of the structure was covered [9]. The importance of appropriate infusate concentrations and coverage of targeted structures for therapeutic efficacy is further highlighted in non human primate studies demonstrating a relationship between intraputaminal levels of GDNF protein and significant behavioral improvements [10,11].

Convection enhanced delivery (CED) has been proposed as a method to maximize infusate distribution [12] and reduce the number of intracerebral injections, therefore decreasing the risks associated to each brain penetration [13]. CED methods have been reported for a number of clinical trials with different degrees of success [1,2,7,3,4,14]. A CED infusion is expected to generate a spherical cloud of infusate emerging from the catheter tip [15], yet a symmetrical sphere does not match the elongated profile of the putamen. Furthermore, as the outer boundaries of the nucleus do not present a barrier to fluid flow, infusion carries the risk of unintentionally affecting neighboring structures. The putamen nucleus is surrounded by white matter tracts (corona radiata, internal capsule, and external capsule) which are known to be more conductive than gray matter [16]. Similarly, the perivascular space of blood vessels near the infusion catheter also provides paths of low resistance and preferred flow for fluids [17]. While these channels are naturally occurring in the brain, the surgical procedures needed for the infusion in themselves can create paths of low fluid resistance, such as the "annulus" surrounding the catheter formed during its insertion and the tract left by the withdrawal of the catheter after infusion [16].

In this report we aimed to evaluate patterns of infusate distribution in the putamen nucleus in order to identify possible pathways of infusate loss and their relative impact to the success of

targeted CED into the postcommisural ventral putamen nucleus. Taking advantage of intraoperative magnetic resonance imaging (IMRI) technology, we obtained three-dimensional maps of gadolinium concentration during the intracerebral infusions, using our previously described method [18]. Thus, we were able to quantify the dose of tracer and its distribution in the brain, tracking the tracer in both, time and space.

Methods

Subjects

Five adult female rhesus monkeys (*Macaca mulatta*) and eight adult female cynomolgous monkeys (*Macaca fascicularis*) were used in this study. Animals were housed individually on a 12-hour light/dark cycle and received food and water *ad libitum*. The animals' diet was supplemented with fruit during daily enrichment. All efforts were made to ameliorate suffering of animals. This study was performed in strict accordance with the recommendations in the Guide for the Care and Use of Laboratory Animals of the National Institutes of Health. The protocol was approved by the Institutional and Animal Care Committee of the University of Wisconsin, Madison (permit #: G00554). Age, weight, and putaminal sizes of each subject are contained in supplementary Table S1.

Surgery and targeting method

Catheters were targeted to the ventral postcommisural right and/or left putamen, approximately 1-2 mm posterior to the coronal plane presenting the anterior commissure using a MRI-compatible external trajectory guide (Navigus, Medtronic Inc., Minneapolis, MN, USA). The planned trajectories were centered laterally at least 5 mm deep within the putamen. The sterile surgical procedure followed our previously published protocol [19]. Briefly, the animal was put under isoflurane (1-3%), its vital signs monitored and placed in a MRI-compatible stereotaxic frame using the coordinates obtained during a baseline MRI. The entry point (identified in the baseline MRI) was located on the surface of the skull. Craniotomies 8 to 12 mm in diameter were drilled at the planned entry area corresponding to the opening of the trajectory guide base. The dura was retracted to expose the brain, and the trajectory guide base was mounted to the skull over the craniotomy. In the MRI suite, a cannula filled with sterile degassed water was inserted into the stem of the trajectory guide. Targeting (3D T1W) MRI scans were taken to position the cannula guide in the anterior-posterior (AP) and mediolateral (ML) planes. When the trajectory angle of the fluid filled cannula was confirmed to be on target, the alignment stem was locked into position, the guiding insert and the remote introducer were placed in the guiding stem and the catheter for the infusion was threaded and fastened to the remote introducers by a locking mechanism.

Infusion

Custom made stepped catheters were used in this project. They consisted of a fused silica shaft with an outside diameter 0.65mm and inside diameter 0.32 mm. A 3 mm length tip with outer diameter 0.36 mm and inner diameter 0.25 mm extended from the end of the shaft. Three variations of the tip design were tested (Table 1): a polyimide open end port with a stylet to close the port during insertion (n=14); the same polyimide tip used without a stylet (n=5); and a microporous-walled tip material with closed end (n=3). As we did not observe major differences in the infusion pathways between these catheter variations, the data of all infusions were considered in the analysis.

Silica infusion lines were used to connect the catheter to 5cc Hamilton gas-tight syringes. The syringes were driven by an MRI-compatible syringe pump (PHD 2000, Harvard Apparatus, Holliston, MA, USA) placed at approximately the same height as the catheter tip.

Line pressure was monitored continuously throughout the infusion. The catheter was introduced into the brain, advancing the remote introducer at approximately 5-7 mm/min.

The infusate was a solution of gadoteridol (2 mMol/L; ProHance, Bracco Diagnostics Inc., Princeton, NJ, USA) and bromophenol blue (0.16 mg/ml; Sigma Aldrich, St Louis, MO, USA) in phosphate buffered saline. A volume of 100μl was infused at an average flow rate of 1.0 μl/min in each infusion. After the infusion was completed, the catheter was left in place for approximately 10-30 minutes before withdrawal. In one case (Cy0279-left) the stylet was replaced to cover the end port before catheter withdrawal.

MRI Acquisition

Imaging was performed in a 3-Tesla GE SIGNA (GE Healthcare; Waukesha, WI) MRI scanner with a custom 3-inch diameter, receive-only surface coil (MR Instruments, Inc. Minneapolis, MN) as previously described [19]. Pre-surgical MRI scans included three dimensional T_1-weighted (T1W) images with an inversion recovery-(IR-) prepped, fast gradient-echo (IR-fGRE) sequence. The scanning parameters were an inversion time (T_I) = 450 ms, repetition time (T_R) = 9.2 ms, echo time (T_E) = 4.1 ms, receiver bandwidth = ±25 kHz. The matrix size was $256 \times 224 \times 128$, 140×105 mm in-plane FOV. The scans produced 0.8 mm thick slices at 0.4 mm spacing, reconstructed in-plane to 0.27×0.27 mm voxels in a scan time of 7:50 minutes. Pre-surgical MRI angiography was obtained using a T1-weighted high resolution spoiled gradient echo (SPGR) sequence with $T_R = 15$ ms, $T_E =$ 3.7 ms, flip angle = 30°, matrix size $256 \times 256 \times 312$, 140mm in-plane FOV, slice thickness = 0.6mm, slice separation = 0.3mm. The slices were reconstructed at 0.27×0.27mm in plane voxels. The acquisition was repeated twice both before and after (5 minutes post) intravenous injection of a single dose of Prohance contrast agent (0.2 ml/kg equivalent to 0.1mmol/kg).

During the infusions, a pair of 3D spoiled gradient echo (SPGR) scans with different flip angles (6° and 34°) was used to map T1 (TR =21 ms, TE = 6 ms, in-plane FOV = 140×105 mm (0.75 phase FOV), matrix = 256×224, 64 contiguous coronal slices each 1.6 or 0.8 mm thick.) A pair was acquired just prior to the start of infusion as a baseline, and then the pair was repeated at approximately 9-minute intervals during the infusion.

MRI Post-Processing

Contrast agent concentration measurements—T1 maps were computed from consecutive pairs of 3D SPGR scans at 6° and 34° flip angles using the variable nutation method [20]. All of the SPGR scans were co-registered prior to T1 map computation to compensate for slight movement of the animal during infusion. Concentration maps were then computed from each pair of scans as described in [18]. Briefly, the equation $1/T1 = 1/T1_0 + R_1*C$, is used, where $T1_0$ is the pre-infusion T1, R_1 is the gadoteridol T1 relaxivity, and C is the concentration. Gadoteridol relaxivity was calibrated by imaging vials of known concentration, and was estimated to be 3.7 milliMoles per Liter-second (mM/L-sec). The minimum concentration that could be reliably estimated by this method was 0.05 mM/L. The total amount of gadoteridol tracer in a region (in nanoMoles) is computed from the concentration maps by summing over the measured concentration at each voxel within the region (in nanoMoles/μl) and multiplying by the volume represented by each voxel (in μl).

Segmentation of the putamen—In each subject, the putamen was delineated by hand from a high resolution T1-weighted scan ($0.27 \times 0.27 \times 0.4$ mm voxel resolution) guided by a rhesus MRI brain atlas [21]. Each voxel in the scan was classified as either 'in' or 'out' of the putamen, resulting in a 3D binary volume identifying the putamen. The putamen segmentation was used to classify each voxel in the concentration maps, and thus to obtain

estimates of the total amount of gadolinium inside and outside of the putamen at each measurement (i.e., at 9 minute time intervals).

MRI angiography processing—MRI angiography was acquired with and without contrast, allowing digital subtraction in order to enhance the signal of the vasculature. The vessels of the NHP putamen are small relative to the imaging resolution. Their identification is further complicated by spatial variations in signal intensity across the images mainly due to RF inhomogeneity of the surface coil. We therefore computed the ratio of the contrast and non-contrast images (rather than the difference), obtaining normalized vascular imagery. The data was windowed to the range 1.15 - 1.3, corresponding to 15-30% signal enhancement in the contrast images. Where classification of vessels was required, a threshold of 1.19 was used to classify vessels in the NHP putamen.

Loss quantification—Based on the putamen segmentation, infusion concentration outside the structure was considered infusate loss and was reported as loss fraction, which is the ratio of the amount classified as loss to the total amount.

Backflow distance—Infusate following the catheter shaft was considered backflow and it was measured from the tip of the catheter to the most proximal point of enhancement along the shaft. Backflow was visible in the T1-weighted MRI usually within a few minutes after the start of the infusion. As the infusion continued, the backflow region became obscured by the growing infusion cloud. Thus, the backflow distance was measured in the first available T1-weighted acquisition after the start of infusion.

Catheter depth measurements—The catheter depth was defined to be the length of catheter lying within the putamen, and it was measured as the distance along the catheter from the tip to the border of the putamen.

Results

In all cases the ventral postcommisural putamen target was reached, as defined in the presurgical planning [19]. Four typical pathways for infusate loss were identified and measured: overflow, perivascular flow, backflow, and catheter tract leakage.

Overflow

Evaluation of T1 MRIs in the coronal, axial, and sagittal planes revealed that early in the infusion, distribution of infusate generally consisted of a symmetric portion, in which the measureable pattern extended a constant distance from the catheter tip, and sometimes had asymmetric portions that partially followed the catheter shaft or an artery previously identified in the baseline angiography. As the infusion continued and passed the 30 µl volume, the pattern of distribution in all 22 infusions went beyond the putaminal borders. The putamen did not appear to offer any particular barrier to this path of loss. However, the onset of leakage past the putamen boundaries did not stop further spread within the putamen; the amount in the putamen continued to increase throughout the infusion.

Over the 22 infusions, we found that all infusions began to show some measureable amount of loss by the time 30 µL were infused. Measured loss for each infusion is given in Table 1. Nine of the 22 infusions had loss of 14% or less after 30 µL of infusion. This limit is not surprising, owing to the narrow width of the NHP putamen. All catheter placements were at most 2.5 mm from the nearest putamen boundary (average 1.6 ± 0.7 mm). In most cases, the volume of tissue containing detectable amounts of tracer was at least 150 µL by this time ($V_d/V_i > 5$). The radius of a 150 µL ball is approximately 3.3 mm, and thus any roughly

spherical distribution would overflow the putamen by the time 30 μL is infused. After excluding four infusions that had backflow loss and eight that had significant perivascular loss (>10%) at 30 μl, ten remaining infusions had dominant overflow losses (R95106-right, R03044-both, R03064-both, Cy0288-right, Cy0298-both, Cy0299-left, Cy0279-left). In these 10 infusions, overflow loss was inversely correlated with catheter tip distance from the nearest putamen boundary at both 30 and 100 μl of infusion (Figure 1A; R^2=0.50, p=0.02).

Cy0298-left (Figure 1B-E) is a typical case in which the catheter was placed in its left ventral postcommisural putamen target, 7 mm deep into the structure (from the tip of the catheter to its point of entry into the putamen). The tip was approximately 1.6 mm from the nearest putamen boundary. At 4 minutes, or 4 μl of infusion, some infusate was observed following the catheter shaft (backflow distance: 6 mm; Figure 1B) yet it remained inside the structure, following a symmetrical elongated shape. At 32 μl, it reaches both the lateral and medial putamen edges, and begins to escape at the medial edge into the globus pallidus (arrow, Figure 1C). Near the end of the infusion (96 μL infused) infusate has crossed the lateral boundary into the external capsule (arrows, Figure 1D). At 32 minutes, about 5% of the measured gadoteridol was lost outside the putamen (Figure 1E). After this time, the rate of loss increased as the infusion reached more of the putamen boundary and entered the adjacent structures, including the globus pallidus and the external capsule. At 96 minutes, the fraction of measured tracer within the putamen fell to 76%. Of the 24% of infusate outside the putamen, approximately 8% was lost into the globus pallidus, and another 8% along the external capsule.

Perivascular Loss

During infusion, patterns of asymmetric flow that resembled blood vessels branching were frequently observed. When the imaging of the infusate pattern was matched to baseline angiography, it confirmed that these asymmetric infusate distributions corresponded to the path of a blood vessel. The putamen nucleus is highly irrigated by branches of the lenticulostriate arteries (mostly rostral and medial putamen) and the anterior choroidal arteries (caudal sections) [22]. In 15 out of 22 infusions, during the first 30 μL of infusion we observed lenticulostriate loss shunting fluid away from the putamen. At this time point, the loss fraction among these 15 cases varied greatly, from 1% to 35%, with five infusions having a perivascular loss of over 20%. The average loss over all 22 infusions was 9.4% ± 10.9%. Table 1 gives the estimated perivascular loss along a lenticulostriate artery after 30 μL of infusion. The perivascular loss measurements were performed at this early time point because once past 30 μL, overflow in the same region in some of the infusions makes it difficult to ascribe a given amount to being along the blood vessel. Infusions performed near the anterior choroid arteries toward the most posterior putamen section also resulted in a similar asymmetric pattern of infusate loss, but these were less common in our catheter trajectories.

Cy0287-right (Figure 2) is an example of flow along a lenticulostriate branch. These vessels typically do not lie within the imaging plane, thus three-dimensional imaging data was re-sliced obliquely at an orientation between the axial and coronal planes in order to observe a portion of the artery near the catheter in a single image. In Figure 2A, such an oblique slice of the brain is shown, 10 minutes after the start of the infusion. The projection of the line of the catheter onto this plane is shown, but the shaft is in fact out of the plane of the image, making approximately a 45 degree angle with the plane shown. The tip of the catheter was centered within the main ball of the infusion. A highly asymmetric flow was observed from the start of the infusion. In Figure 2B, the co-registered angiography image is overlaid, showing that the asymmetry correlates with the path of a lenticulostriate artery. As the infusion continued, there was expansion about the main infusion ball around the catheter, and about the asymmetric projection along the lenticulostriate path (Figure 2C). The flow

followed the perivascular space for a limited distance, and then spread out "cylindrically" from an annular source of fluid surrounding the vessel. In this case, the fraction of loss out of the putamen continued to increase (Figure 2D) when the boundary of the putamen was reached.

Backflow

Asymmetric infusate distribution following the catheter shaft was observed during all infusions. Yet, there were only four cases (Cy0140-left, Cy0295-right, R5008-right, Cy0288-left) out of the 22 infusions observed in which the backflow reached or extended beyond the top boundary of the putamen. In these four cases, the fraction of total dose lost along the backflow pathway increased over the first 30-60 minutes to a peak value and remained relatively stable after 60 minutes (Table 1). In three out of the four cases (Cy0295-right, R5008-right, Cy0288-left), the fractional loss was clustered close to 35% on the average, ranging from 30 to 40%. In the fourth case (Cy0140-left) high backflow loss was 70% which was atypical for the device and low flow rate protocol used (Figure 3). The catheter was placed 6mm deep in the putamen, with the tip 2mm from the nearest putamen boundary (Figure 3A). The backflow was visible in MRI within 9 minutes from the start of the infusion (Figure 3B). The backflow distance along the catheter shaft was 16mm, far beyond the top boundary of the putamen. About 70% of the measured gadoteridol was lost into the white matter surrounding the catheter, superior to the putamen (Figure 3C, D). The fractional loss stabilized at this rate after about 30 minutes of infusion. While the loss was considerable, most of the remaining 30% of the infusate concentration remained within the putamen, and the total dose in the putamen increased throughout the infusion (albeit at a reduced rate). Thus, continued infusion also continues to fill the putamen at this fraction while losses from other causes are not present.

A certain amount of variability in backflow distance arises from variation in biological properties. The average backflow distance (± standard deviation) over all 22 infusions was 5.0 ± 3.4mm, ranging from 2–16 mm. However, backflow that exits the putamen is affected by the tissue properties of the white matter outside the putamen. For the 18 infusions in which the backflow remained within the putamen, average backflow distance was 3.8 ± 1.0mm. On average, the depth of catheter placement within the putamen was 6.2 ± 1.1mm, which was usually sufficient to avoid backflow out of the putamen at the low flow rate (1 μL/min) employed.

Leakage into the Catheter Tract

Ten to 30 minutes after the infusions were completed, the catheters were extracted (Table 1). Subsequent imaging revealed leakage of tracer along the full length of the catheter tract in all cases (Table 1). In one case (Cy0279-left) the stylet was replaced just before catheter withdrawal, and yet infusate was still observed in the catheter tract. Eleven of the infusions had imaging that allowed quantitative measurement of the amount in the catheter track (R03044-right, R03064-right, Cy0286-left, Cy0287-right, Cy0298-left, Cy0299-left, Cy0279-left, Cy0288-left, Cy0295-left, Cy0299-right, and Cy0279-right). The mean measured amount in the catheter track was $1.6\% \pm 0.7\%$ of the total infused amount. The loss did not vary significantly with the waiting time before withdrawal in the 10-30 minute range (Figure 4A; R^2=0.08, p=0.40).

Cy0286-left (Figure 4B,C) is an example of leakage into the catheter tract after waiting 16 minutes before retracting the catheter. Tracer appeared to be drawn up the tract by the catheter during its withdrawal. MRI measurement of the gadolinium deposited in the track in this example yielded an estimate of 3.6 nM, which is the amount of gadolinium contained in 1.8 μl of infusate, 1.8% of the infused amount.

Conclusions and Discussion

This study demonstrates, during CED into ventral postcommisural putamen nucleus of macaque monkeys, four main paths for infusate loss outside of the target area: overflow, perivascular flow, backflow, and catheter tract leakage. It also demonstrates the value of IMRI for replicable intracerebral targeting; 22 of 22 cases have catheter placements in the planned region of interest. Quantification of the magnitude of the loss by IMRI monitoring suggests that infusate volume and regional vasculature are the main factors for infusate loss in the non human primate brain and provide insight of possible issues that can affect the success of human studies.

It could be argued that the data obtained in monkeys has limited application to the larger human brain. While it is true that the human putamen is approximately six times larger in volume than our average monkey, it has a more elongated shape, further complicating a strategy of coverage via a single spherical infusion. The rhesus putamen is not much narrower in the postcomissural region than that of the human [23]. This implies that for clinical trials, similar to our study, it will be difficult to place a catheter more than a few millimeters from the nearest lateral boundary and thus overflow loss from the human putamen will occur before high coverage of the nucleus is reached. Considering these limitations, it seems that multiple inoculations sites are needed to reach therapeutic coverage of the putamen.

Some investigators have proposed that perivascular flow is a major mechanism responsible for intracerebral distribution of infusates [24]. In our study, blood vessels were associated with asymmetric infusate distributions that were an apparent pathway of loss. Blood vessel distribution limits the selection of sites for optimal catheter position, as they should be avoided in order to limit perivascular leakage. In non human primates, the largest vessels were usually found in the anterior half of the putamen, whereas in humans, the large vessels are more widely distributed [22], which may make them more difficult to avoid.

Previous studies have identified backflow as having a potentially important role in loss and misdistribution of infusate. Although we observed some amount of backflow in all of the cases, the loss along this path was only significant in four cases in which the backflow extended past the putamen boundary into the adjacent corona radiata. The intraputaminal depth of the catheter was a variable that for our study had to be adjusted by subject and seemed to affect the capacity to contain the backflow inside the structure. The greater height of the human putamen along the usual superior/inferior catheter trajectory should allow for deeper catheter placements, and thus lowered risk of backflow loss. We deliberately selected a low flow rate (1 μl/min) that limited the chance of backflow out of the putamen in our study. However, some prior and proposed human trials have used significantly larger flow rates and catheter diameters than used in our animal study. Both factors tend to increase the backflow distance and with it the risk of backflow loss into the white matter. An axial catheter trajectory passing through the frontal sinuses was previously used in a PD clinical trial using fetal tissue for cell replacement [25]. This approach is not commonly used due to its of damage to the frontal lobe, but it might have a geometric advantage, in that a catheter could be inserted along the long axis of the putamen and take advantage of the elongation of the distribution due to backflow. It should be noted that it is not feasible to test the frontal insertion angle in macaques due to their extensive skull bone mass at the required entry point.

Catheter tract leakage of infusate was observed along the path of the withdrawn catheter in all cases. This pattern was found even after waiting up to 30 minutes post infusion before retracting the catheter. This loss is likely to occur during human infusions, especially if the

catheter is removed shortly after infusion. While the infusate loss in monkeys was limited to a few microliters, it should be taken into consideration in the case of delivering gene therapy, as the presence of viral vectors may induce overtime undesired accumulation of proteins in non-target areas. We have observed that if the stylet is replaced after infusion in order to seal the catheter from leakage during withdrawal, the loss into the track is not reduced. Thus, the source of the infusate must be from the infusate already in the tissue. The rapid appearance of this leakage indicates that is it pressure-driven, rather than diffusing. This could be due to a vacuum created from the catheter withdrawal. Alternately, the pressure of convection tends to expand the tissue during infusion, and the tissue relaxing back to its original shape may provide some of the convective pressure. Further delayed catheter removal in acute infusion systems may mitigate this loss and add safety to the infusion protocol. However, in our studies, a delay of up to 30 minutes was insufficient to mitigate the effect.

The characteristics of the infusate should be considered when analyzing distribution patterns. To facilitate our analysis we utilized in all our infusions the same gadoteridol infusate solution. Gadoteridol has a molecular weight of 558.7 Da. The use of proteins or viral vectors of greater molecular size, electric charge, as well as concentration/vector titer and different biological properties (such as receptor affinity) will have to be considered when planning intraputaminal deliveries.

To conclude, our analyses demonstrate that after controlling for targeting, catheter type, infusion rate and infusate characteristics, the main issues during surgical planning are the identification of appropriate infusate volume that matches the target area, as well as mapping the regional vasculature as it may become a pathway for infusate loss. Most importantly, these results underscore the significance of presurgical planning for catheter placement and infusion methods as well as the value of imaging guidance to ensure targeting accuracy.

Supplementary Material

Refer to Web version on PubMed Central for supplementary material.

Acknowledgments

References

1. Lang AE, Gill S, Patel NK, Lozano A, Nutt JG, Penn R, Brooks DJ, Hotton G, Moro E, Heywood P, Brodsky MA, Burchiel MA, Dalvi KP, Scott B, Stacy M, Turner D, Wooten VG, Elias WJ, Laws ER, Dhawan V, Stoessl AJ, Matcham J, Coffey RJ, Traub M. Randomized controlled trial of intraputamenal glial cell line-derived neurotrophic factor infusion in Parkinson disease. Ann Neurol. 2006; 59(3):459–66. [PubMed: 16429411]

2. Marks WJ, Bartus RT, Siffert J, Davis CS, Lozano A, Boulis N, Vitek J, Stacy M, Turner D, Verhagen L, Bakay R, Watts R, Guthrie B, Jankovic J, Simpson R, Tagliati M, Alterman R, Stern M, Baltuch G, Starr PA, Larson PS, Ostrem JL, Nutt J, Kieburtz K, Kordower JH, Olanow CW. Gene delivery of AAV2-neurturin for Parkinson's disease: a double-blind, randomized, controlled trial. Lancet Neurol. 2010; 9(12):1164–72. [PubMed: 20970382]

3. Nutt JG, Burchiel KJ, Comella CL, Jankovic J, Lang AE, Laws J, ER, Lozano AM, Penn RD, Simson J, RK, Stacy M, Wooten GF. Randomized, double-blind trial of glial cell line-derived neurotrophic factor (GDNF) in PD. Neurology. 2003; 60(1):69–73. [PubMed: 12525720]

4. Patel NK, Bunnage M, Plaha P, Svendsen CN, Heywood P, Gill SS. Intraputamenal infusion of glial cell line-derived neurotrophic factor in PD: a two-year outcome study. Ann Neurol. 2005; 57(2): 298–302. [PubMed: 15668979]

5. Richardson RM, Kells AP, Rosenbluth KH, Salegio EA, Fiandaca MS, Larson PS, Starr PA, Martin AJ, Lonser RR, Federoff HJ, Forsayeth JR, Bankiewicz KS. Interventional MRI-guided putaminal delivery of AAV2-GDNF for a planned clinical trial in Parkinson's disease. Mol Ther. 2011; 19:1048–57. [PubMed: 21343917]

6. Slevin JT, Gerhardt GA, Smith CD, Gash DM, Kryscio R, Young B. Unilateral Intraputamenal GDNF improves bilateral motor functions in patients with Parkinson's disease. J Neurosurg. 2005; 102:216–22. [PubMed: 15739547]

7. Marks WJ, Ostrem JL, Verhagen L, Starr PA, Larson PS, Bakay RAE, Taylor R, Cahn-Weiner DA, Stoessl AJ, Olanow CW, Bartus RT. Safety and tolerability of intraputaminal delivery of CERE-120 (adeno-associated virus serotype 2—neurturin) to patients with idiopathic Parkinson's disease: an open-label, phase I trial. Lancet Neurol. 2008; 7(5):400–8. [PubMed: 18387850]

8. Morrison PF, Lonser RR, Oldfield EH. Convective delivery of glial cell line-derived neurotrophic factor in the human putamen. J Neurosurg. 2007; 107:74–83. [PubMed: 17639877]

9. Bartus RT, Herzog CD, Chu Y, Wilson A, Brown L, Siffert J, Johnson J, EM, Olanow CW, Mufson EJ, Kordower JH. Bioactivity of AAV2-neurturin gene therapy (CERE-120): differences between Parkinson's disease and nonhuman primate brains. Mov Disord. 2011; 26(1):27–36. [PubMed: 21322017]

10. Emborg ME, Moirano J, Raschke J, Bondarenko V, Zufferey R, Peng S, Ebert AD, Joers V, Roitberg B, Holden JE, Koprich J, Lipton J, Kordower JH, Aebischer P. Response of aged parkinsonian monkeys to in vivo gene transfer of GDNF. Neurobiol Dis. 2009; 36:303–11. [PubMed: 19660547]

11. Kirik D, Georgievska B, Björklund A. Localized striatal delivery of GDNF as a treatment for Parkinson disease. Nat Neurosci. 2004; 7(2):105–10. [PubMed: 14747832]

12. Bobo RH, Laske DW, Akbasak A, Morrison PF, Dedrick RL, Oldfield EH. Convection-enhanced delivery of macromolecules in the brain. Proc Natl Acad Sci U S A. 1994; 91:2076–80. [PubMed: 8134351]

13. Kimmelman J, Duckworth K, Ramsay T, Voss T, Ravina B, Emborg M. Risk of surgical delivery to deep nuclei: a meta-analysis. Mov Disord. 2011; 26(8):1415–21. [PubMed: 21574186]

14. Sampson JH, Archer G, Pedain C, Wembacher-Schroder E, Westphal M, Kunwar S, Vogelbaum MA, Coan A, Herndon JE II, Raghavan R, Brady ML, Reardon DA, Friedman AH, Friedman HS, Rodriguez-Ponce MI, Chang SM, Mittermeyer S, Croteau D, Puri RK. Poor drug distribution as a possible explanation for the results of the PRECISE trial. J Neurosurg. 2010; 113(2):301–9. [PubMed: 20020841]

15. Morrison PF, Laske DW, Bobo H, Oldfield EH, Dedrick RL. High-flow microinfusion: tissue penetration and pharmacodynamics. Am J Physiol. 1994; 266:R292–305. [PubMed: 8304553]

16. Morrison PF, Chen MY, Chadwick RS, Lonser RR, Oldfield EH. Focal delivery during direct infusion to brain: role of flow rate, catheter diameter, and tissue mechanics. Am J Physiol. 1999; 277:R1218–29. [PubMed: 10516265]

17. Krauze MT, Saito R, Noble C, Bringas J, Forsayeth J, McKnight TR, Park J, Bankiewicz KS. Effects of the perivascular space on convection-enhanced delivery of liposomes in primate putamen. Exp Neurol. 2005; 196(1):104–11. [PubMed: 16109410]

18. Brady ML, Raghavan R, Chen Z, Broaddus W. Quantifying Fluid Infusions and Tissue Expansion in Brain. IEEE Trans Biomed Eng. 2011; 58(8):2228–2237.

19. Emborg ME, Joers V, Fisher R, Brunner K, Carter V, Ross C, Raghavan R, Brady M, Raschke J, Kubota K, Alexander A. Intraoperative intracerebral MRI-guided navigation for accurate targeting in nonhuman primates. Cell Transplant. 2010; 19:1587–97. [PubMed: 20587170]

20. Deoni S, Peters T, Rutt B. Determination of optimal angles for variable nutation spin-lattice, T1, and spin-spin, T2, relaxation times measurement. Mag Reson Med. 2004; 51:428–433.

21. Saleem, KS.; Logothetis, NK. A Combined MRI and Histology Atlas of the Rhesus Monkey Brain in Stereotaxic Coordinates. Academic Press; London: 2006.

22. Donzelli R, Marinkovic S, Brigante L, de Divitiis O, Nikodijevic I, Schonauer C, Maiuri F. Territories of the perforating (lenticulostriate) branches of the middle cerebral artery. Surg Radiol Anat. 1998; 20:393–8. [PubMed: 9932322]

23. Yin D, Valles F, Fiandaca M, Forsayeth J, Larson P, Starr P, Bankiewicz K. Striatal volume differences between non-human and human primates. J Neurosci Methods. 2009; 176(2):200–5. [PubMed: 18809434]

24. Hadaczek P, Yamashita Y, Mirek H, Tamas L, Bohn MC, Noble C, Park JW, Bankiewicz K. The "perivascular pump" driven by arterial pulsation is a powerful mechanism for the distribution of therapeutic molecules within the brain. Mol Ther. 2006; 14:69–78. [PubMed: 16650807]

25. Freed C, Greene P, Breeze R, Tsai WY, DuMouchel W, Kao R, Dillon S, Winfield H, Culver S, Trojanowski J, Eidelberg D, Fahn S. Transplantation of embryonic dopamine neurons for severe Parkinson's disease. N Engl J Med. 2001; 344:710–719. [PubMed: 11236774]
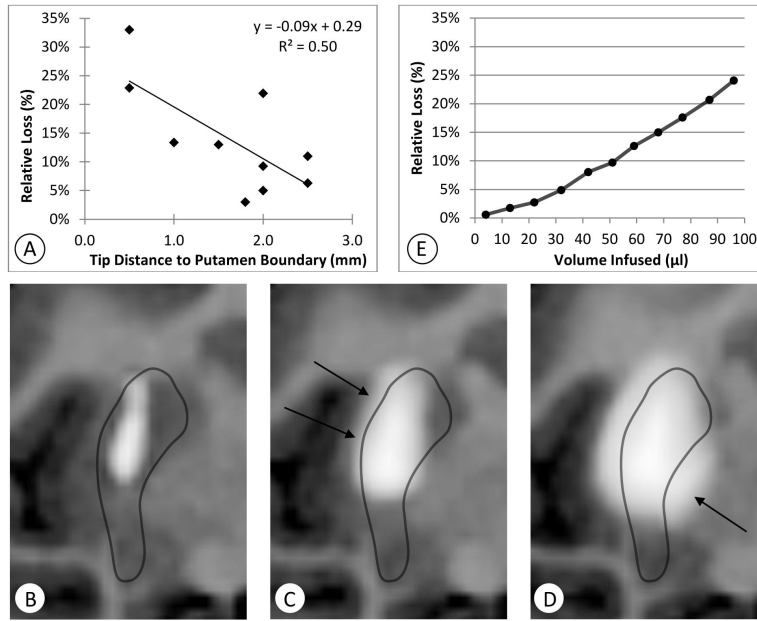
Figure 1.
Illustration of overflow loss. A: Correlation between the distance of the catheter tip to the nearest putamen boundary and the fraction of measured gadolinium outside the putamen after 30 µl of infusion for 10 infusions dominated by overflow. B–D: Quantitative T1 maps (negated) for a specific example (Cy0298-left) centered at the catheter tip during the infusion of 100µl (infusion rate: 1µl/min), show infusate overflow out of the putamen over time. B: 6 mm of backflow contained within the putamen was detected a few minutes after the start of the infusion. C: At 32 minutes infusate begins to move past the medial edge of the putamen. D: At the end of the 100-minute infusion the tracer begins to spread into the external capsule on the lateral side of the putamen (arrows). E: Plots of the computed amount of tracer outside the putamen divided by the total measured amount at approximately 10 minute intervals (Cy0298).
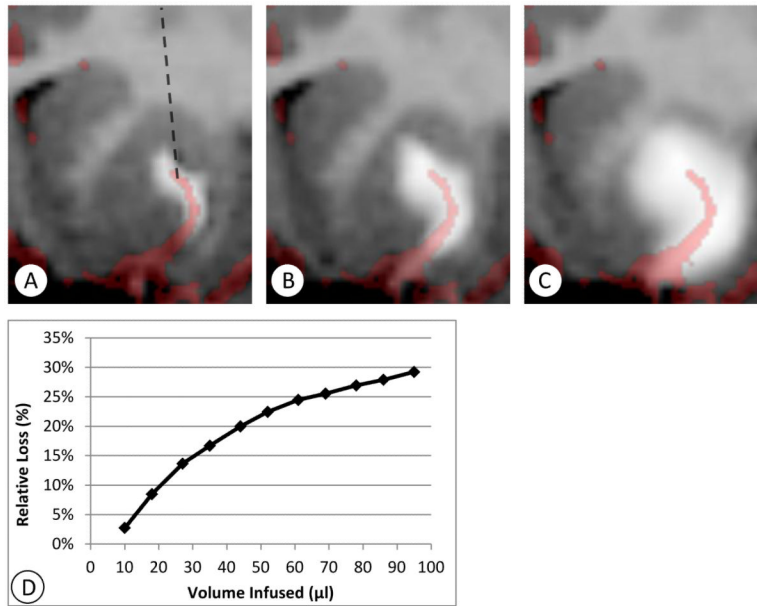
Figure 2.
Example of perivascular loss (Cy0287-right). T1 maps (negated) were re-sliced obliquely at approximately 45 degrees between the coronal and axial planes, so that an artery located near the catheter tip is visible. MR angiography is co-registered and overlaid, illustrating the location of the nearby artery and the correlation of the asymmetric flow to the path of the artery. A: Ten minutes after the start of infusion the highly asymmetric flow is visible. The projection of the catheter into this oblique plane is shown in A (dashed line). The catheter itself lies in the coronal plane. The infusion continues to expand laterally as the infusion proceeds, as shown in B: 27 minutes after the start of infusion, and C: 95 minutes after the start of infusion.
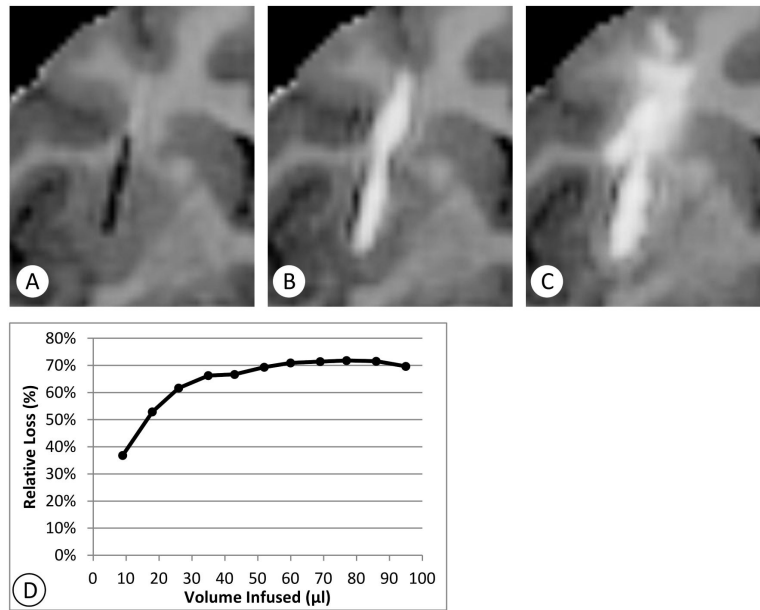
Figure 3.
Extreme example of backflow loss (Cy0140-left). Coronal T1-maps (negated) centered at the catheter position illustrate that backflow along the catheter shaft can be a major cause of infusate loss out of the putamen. In this extreme example, about 70% of the infusate flows outside of the nonhuman primate putamen. A: Shows the pre-infusion catheter position. B: backflow is clearly developed outside the putamen, 13 mm from the catheter tip, at 18 minutes. C: Most of the infusate flows out the top of the putamen and spreads through the frontal white matter tracts above the putamen as the infusion continues.
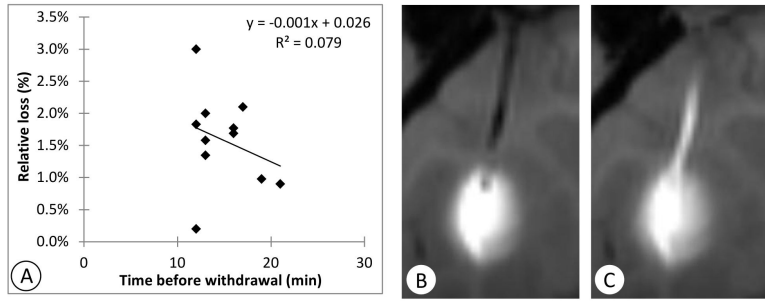
Figure 4.
Illustration of leakage into the catheter tract. A: Correlation between time before catheter withdrawal and fraction of infusate found to leak into the catheter track shows little correspondence. Coronal T1-weighted MRI images of one example (Cy0286-left) B: at the end of infusion before withdrawing the catheter and C: 30 minutes after withdrawal of the catheter.

Table 1

Infusate distribution measurements for all 22 infusions. 'Cath.' refers to the catheter tip type:VT, valve tip (stylet end port); VT*, valve tip, occluded before retrieval; NS, no stylet end port; FM = fiber mesh. Side: r, right; l, left. Depth refers to the distance to from the catheter tip to the nearest putamen boundary. Backflow is the extent of tracer reflux visible along the catheter shaft visible 10 minutes after the start of the infusion. Withdrawal refers to the time end of infusion and removal of the catheter. Loss fractions (perivascular, backflow, and total) are the fraction of the total measured amounts of infusate that are outside the putamen

Animal	Side	Cath.	Depth (mm)	Tip dist. (mm)	Backflow (mm)	Withdrawal (min)	Loss Fraction @ 30µl			Loss Fraction @ 100µl	
							Perivascular	Backflow	Overall	Backflow	Overall
R91070	r	VT	5.0	2.5	5.0	10	16%		39%		66%
R95106	r	VT	6.0	2.5	2.0	12	3%		6%		24%
R03044	r	VT	6.5	2.5	4.0	13	8%		11%		30%
R03044	l	VT	6.5	2.0	4.0	13	7%		22%		38%
R03064	r	VT	8.0	1.0	3.0	12	6%		13%		37%
R03064	l	VT	5.0	2.0	3.0	12	2%		9%		34%
Cy0140	l	VT	6.0	2.5	13.0	12	1%	62%	67%	70%	76%
Cy0286	l	VT	4.5	0.5	3.0	16	20%		34%		52%
Cy0287	r	VT	7.0	1.5	3.0	19	14%		18%		40%
Cy0288	r	VT	5.5	0.5	3.5	16	0%		23%		40%
Cy0295	r	VT	5.0	1.5	8.0	17	0%	7%	14%	43%	51%
Cy0298	l	VT	7.0	2.0	6.0	13	0%		5%		24%
Cy0299	l	VT	6.5	0.5	5.0	12	8%		33%		56%
Cy0279	l	VT*	7.0	1.5	5.0	16	0%	21%	13%	34%	46%
R05008	r	NS	7.0	2.0	16.0	15	0%		32%		46%
Cy0286	r	NS	7.0	0.7	3.5	14	20%		42%		52%
Cy0287	l	NS	9.0	1.5	3.0	18	35%		41%		56%
Cy0288	l	NS	4.5	2.0	6.0	17	0%	8%	20%	29%	49%
Cy0295	l	NS	5.0	1.5	3.0	21	31%		33%		51%
Cy0298	r	FM	6.0	1.8	4.0	30	0%		3%		21%
Cy0299	r	FM	5.5	1.5	3.5	13	25%		30%		47%
Cy0279	r	FM	6.0	1.0	4.0	12	11%		13%		40%
Mean ± SD			6.2 ± 1.1	1.6 ± 0.7	5 ± 3.4		9.4% ± 10.9		24% ± 16		44% ± 13